

Conductive polymer-inorganic hybrid materials through synergistic mutual doping of the constituents

Weike Wang^{†,‡,§}, *Chaoqiu Chen*[‡], *Christopher Tollan*[†], *Fan Yang*[†], *Mikel Beltrán*[†], *Yong Qin*^{‡,*},
and *Mato Knez*^{†,||,*}

[†]CIC nanoGUNE, Tolosa Hiribidea, 76, 20018 Donostia-San Sebastian, Spain

[‡]State Key Laboratory of Coal Conversion, Institute of Coal Chemistry, Chinese Academy of Sciences, Taiyuan, 030001, China

[§]University of Chinese Academy of Sciences, Beijing, 100049, China

^{||}IKERBASQUE, Basque Foundation for Science, 48011 Bilbao, Spain

*E-mail: qinyong@sxicc.ac.cn (Y. Qin); m.knez@nanogune.eu (M. Knez)

ABSTRACT: Polymer matrix based inorganic-organic hybrid materials are at the cutting edge of current research for their great promise to merge properties of soft and hard solids in one material. Infiltration of polymers with vapors of reactive metal organics is a pathway for post-

synthetic blending of the polymer with inorganic materials. Here we show that this process is also an excellent method for fabricating conductive hybrid materials. Polyaniline (PANI) was infiltrated with ZnO and the initially insulating polymer was converted to a PANI/ZnO hybrid with conductivities as high as 18.42 S/cm. The conductivity is based on a synergistic effect of the constituting materials where the inorganic and the polymeric fractions mutually act as dopants for the counterpart. The process temperature is a very important factor for a successful infiltration and the number of applied infiltration cycles allows tuning the level of conductivity of the resulting PANI/ZnO.

KEYWORDS: multiple pulsed infiltration, synergistic mutual doping, conductive polymer, polyaniline, ZnO, atomic layer deposition

INTRODUCTION

Since copper-like electrical conductivities were reported in polyacetylene films in the late 1970s,¹ considerable research efforts have been devoted to enhancing the conductivities of various polymers and their integration into a variety of devices.²⁻⁷ Polyaniline (PANI) belongs to the most prominent intrinsically conducting polymers (ICPs) and has enjoyed great attention in research for decades, not at least for its facile polymerization, simple doping/dedoping processes and rich redox chemistry.⁸ The insulating emeraldine base (EB), which is used in this work, can be converted to the conductive emeraldine salt (ES) by doping it with inorganic protonic acids,^{9,10} organic acids,¹¹ alkali metal salts,¹² Lewis acids,^{13,14} or transition metal salts.¹⁵ Also, some metal oxides such as SnO₂, ZnO, etc. have been successfully used as dopants.^{16,17}

Insertion of inorganic materials into polymers is often applied for fabricating composites or hybrid materials with enhanced mechanical, optical, or electronic properties.¹⁸⁻²⁴ However, most incorporation processes are carried out in solution, often with negative consequences for the polymer morphology, structure and/or purity. A very recently developed solvent-free technique for blending polymers with inorganics relies on multiple pulsed infiltration (MPI), which is a modified version of atomic layer deposition (ALD).²¹ The characteristic sequential pulse/purge sequence of two or more precursors that ensures self-limited coatings in ALD is complemented with an extended intermittent exposure time to ensure sufficient time for the precursors to diffuse into a polymeric substrate and chemically bind before purging the excess precursor and byproducts. The sequence is otherwise repeated (cycled) in the same way as ALD. The infiltrated metal organic precursors allow chemical reactions in the subsurface area of the substrate, which a solvent would otherwise shield, resulting in a new hybrid material (**Figure 1**). Our group has explored the infiltration of a number of biopolymers, including spider silk,²² collagen,²³ and cellulose,²⁴ mainly targeting their mechanical properties. Given that the infiltration is accompanied with a chemical modification of the substrate, the electronic properties of the substrate may also be altered. Here, we demonstrate that the MPI process for ZnO, applying the two typical ALD precursors diethylzinc (DEZ) and water (H₂O), is an outstanding strategy for doping PANI. The components of the resulting hybrid material mutually dope each other with the resulting conductivities greatly outperforming those of conventionally doped PANI.

EXPERIMENTAL SECTION

Synthesis of polyaniline nanofibers. The synthesis of PANI nanofibers was carried out by rapid mixing polymerization as reported in literature.¹⁰ All chemicals were analytical grade and used as received. Typically, aniline (3.2 mmol, 0.291 ml) and ammonium peroxydisulfate (0.8 mmol, 0.183 g) were dissolved in 10 ml 1M HCl each. The two solutions were rapidly mixed at room temperature (20 °C) and immediately shaken to ensure sufficient mixing. After 12 h the polymerization was concluded and the resulting 1M HCl doped polyaniline was collected by filtration and repeatedly washed with 1M HCl until the filtrate became colorless. Thereafter the polymer was dried in vacuum at 50 °C. Dedoped polyaniline was obtained by treating the PANI/1M HCl with aqueous ammonium hydroxide (5 %) for 1h and subsequent washing with deionized water until the filtrate became neutral. The dedoped PANI was dried in vacuum at 60 °C. PANI films were prepared by drop-casting its aqueous dispersion (200 µl) on (1.3×1.3 cm²) glass slides. The glass substrates were pre-cleaned with acetone, deionized water (DI), and isopropanol in that sequence. The resulting samples were dried in an oven at 60 °C for 12 h.

Multiple pulsed infiltration (MPI). The multiple pulsed infiltration process was done in an ALD reactor (Savannah S100, Cambridge Nanotech Inc). Dedoped PANI films on glass slides were placed into the ALD chamber and dried at 155 °C in vacuum environment (20 mTorr) with a steady N₂ gas stream (50 sccm) for 2 h. Diethyl zinc (DEZ, Strem Chemicals, 99.99%) and purified H₂O were used as sources for Zn and oxygen, respectively. Each cycle was composed of a pulse, exposure, and purge sequence for each precursor. One cycle of the process was as follows: the precursor DEZ was pulsed into the reaction chamber for 0.08 s and held in the reaction chamber for 120 s, followed by a 60 s purge step to remove excess DEZ. In the same manner, the pulse (0.018 s)/exposure (120 s)/purge (60 s) sequence of water was applied. This DEZ/water cycle was repeated as many times as indicated in the sample assignment. As delivery

and purge gas N₂ was used. The reaction temperature was 155 °C, and the base pressure of the reactor was 50 mTorr.

Characterization. Fourier-transform infrared (FTIR) spectra of the samples were recorded between 750 and 1680 cm⁻¹ with a FT-IR Spectrometer (PerkinElmer, Frontier). Morphology examination of the samples was done with a scanning electron microscope (FEI, Quanta 250 FEG) at 10 kV. Thickness measurements were done with cross-sectional FEG-SEM. Raman spectroscopy at 532 cm⁻¹ exciting wavelength was performed with a Raman microscope (Alpha 300S, WITec). The laser power was kept below 0.7 mW in order to avoid sample degradation. X-ray diffraction (XRD) analysis was carried with a powder diffractometer (X'pert, PANalytical with 45 kV, 40 mA) with Ni-filtered Cu K α radiation. XPS experiments were conducted using a Phoibos photoelectron spectrometer equipped with an Al K α X-ray source (12 mA, 8.33 kV) as the incident photon radiation, and the spectra were standardized using the C 1s peak at 284.6 eV. TEM images and EDS analysis was carried out with a FEI titan microscope using 300 kV in STEM mode and an EDAX SDD detector. The FIB used for lamellae preparation was a dual beam Helios Nanolab 450S from FEI. FIB lamellae were prepared from a Si wafer with the PANI fibers deposited on it and after the entire wafer had undergone ZnO MPI treatment. The block was extracted by standard methods using a Pt electron beam deposition to initially protect the sample surface before any ion beam deposition was carried out. The block was thinned to transparency on a copper "Omniprobe" grid using a 5 kV gallium ion beam at 8 pA for final surface preparation. The conductivities of the thin films were measured using a home-built four-point probe setup with a source measurement unit (Keithley 2611). For each experiment 4 or 5 individual samples were tested for each MPI process cycle number. The resulting conductivity, σ , was calculated according to the formula,

$$\sigma = \ln 2(I / \pi d V) \quad (1)$$

where I is the current, V is the voltage and the d is the polymer film thickness.

RESULTS AND DISCUSSION

We fabricated PANI films supported on glass slides and treated them by the MPI process. We infiltrated samples applying short and long exposure times and also fabricated samples with ZnO coatings for comparison. For the latter case an initial layer of Al₂O₃ was pre-deposited, which served as infiltration barrier for the DEZ. Lastly, we surveyed the influence of varying the infiltration cycle numbers. The resulting conductivity values were compared to undoped and HCl-doped PANI.

Figures 2a and **2b** show the room temperature I - V curves of the various PANI samples with similar thicknesses (7 ~ 10 μm), characterized by linear, ohmic behavior. The electrical conductivities of the samples were calculated from the slopes of the I - V plots and are shown in **Figure 2c** and in **Table S1** (supporting information). As expected, untreated PANI thin films showed no noteworthy conductivity. After doping with HCl the conductivity rose from less than 10⁻¹⁰ S/cm to 8.23x10⁻² S/cm. PANI coated with an Al₂O₃ infiltration barrier and an additional ZnO film showed conductivities in the order of 10⁻⁴ S/cm, which can be attributed to the ALD-deposited ZnO that intrinsically shows some level of conductivity.²⁵ A ZnO infiltration with short exposure times of 8 s yielded conductivities similar to the HCl-doped case. The exposure times are correlated with the infiltration depth, thus extended exposure times promised a better performance. Indeed, upon extending the exposure time to 120 s, the conductivities of the HCl-doped sample were outperformed by more than 2 orders of magnitude. Further improvement was

achieved by altering the number of infiltration cycles. Peak values up to 18.42 S/cm were achieved with 600 cycles. Note that the measured conductivities are significantly higher than those (up to 6.8×10^{-3} S/cm) of PANI/ZnO nanocomposites produced with competing approaches.¹⁷ A further increase of the cycle number towards 700 and 900 lowered the conductivities, which might be due to the increasing dominance of the growing external ZnO coatings. It is worth noting that the PANI/ZnO samples were temporally very stable. Upon exposure to laboratory air for 6 months, the conductivities of PANI/ZnO (600 cycles) decreased by a factor of 3 to 4 only, that is, from 18.42 S/cm to 5.67 S/cm (supporting information, **Figure S1**).

The observation that both pre-coating PANI with an infiltration barrier and variation of the exposure times greatly affect the conductivity values implies that the observed conductivity is not resulting from the PANI or ZnO only, but a synergy of the involved materials is of crucial importance. From the morphological point of view, the polymer did not show obvious changes after infiltration. In **Figure 3** scanning electron micrographs (SEM) of PANI nanofibers before and after infiltration with ZnO (200 cycles) are shown. Only slight variations in the fiber diameters resulting from unavoidable surface-deposited ZnO upon infiltration are seen. Transmission electron microscopy (TEM) and energy dispersive X-ray spectroscopy (EDX) scans of cross-sectioned fibers showed a significant presence of Zn in the bulk of the material. The ZnO coating may contribute to the conductivity of PANI by allowing an electron hopping mechanism in principle, but given the large differences observed from the coated and infiltrated samples, it is more likely that the Zn interacts with the functional groups of the polymer in some way that is beneficial for electron conduction. Such a scenario is also favored by the HRTEM and SAED analyses shown in the supporting information in **Figure S2**. The interplanar spacings,

as measured from SAED patterns, were 0.17 nm, 0.19 nm and 0.21 nm, corresponding to the (440), (431), and (332) planes of the c-zinc nitride structure.²⁶ Further identified interplanar spacings of 0.15 nm and 0.21 nm correspond to the (103) and (101) planes of ZnO.^{27,28} The HRTEM image shows the formation of crystallites within the polymer. Those form a network with gaps on the nanometer or subnanometer scale between the crystallites. Thus it can be assumed that the formation of -Zn-N- or -N-Zn-O- bonds is an influencing factor for the conductivity of the resulting hybrid material.

The chemical functionalities in PANI, which allow binding with metal ions, are in the first instance the amine (-NH) and imine (-N=) groups. In typical infrared spectra, the bands at 1593 cm^{-1} (quinoid C=N stretching), 1300 cm^{-1} (N-H bending), 1220 cm^{-1} (benzenoid C-N stretching) and 829 cm^{-1} (out-of-plane C-H bending) are assigned to the EB structure. We performed an infiltration process with 5 cycles only in order to minimize the amount of surface deposited ZnO and in this way enable observation of the chemical changes in the polymer. **Figure 4a** shows that infiltration at temperatures below 100 °C did not affect the aforementioned peaks. A stepwise increase of the process temperature from 120 °C to 180 °C resulted in the bands at 1593 cm^{-1} and 1220 cm^{-1} shifting blue and the bands at 1300 cm^{-1} and 829 cm^{-1} shifting red. Obviously a thermally activated chemical reaction between the polymer and the precursor takes place, which at temperatures equal or above 155 °C becomes pronounced. The band shifts at 1220 cm^{-1} and 1300 cm^{-1} are of importance as they indicate the formation of C-N⁺.²⁹ Note that earlier reported PANI/ZnO composites showed opposite (blue) shift of the bands at 1300 cm^{-1} and 829 cm^{-1} , while the band at 1220 cm^{-1} did not shift.¹⁷ The impact of further processing parameters on the chemistry can be seen in **Figure 4b**. The peaks at 1300 cm^{-1} and 829 cm^{-1} of the control sample (black) are of particular interest. Their shift is a signature for a fractional conversion of quinoid

to benzenoid units as a result of DEZ reacting with amine and imine groups of PANI. Stronger shifts indicate an increased degree of charge delocalization in the PANI backbone, which is most pronounced after infiltration with extended exposure times (red). Pre-deposition of Al₂O₃ appears effective for prevention of infiltration, since neither the spectra of the Al₂O₃ coated (cyan) nor the subsequently ZnO-processed (magenta) samples show significant changes.

Raman spectra (**Figure 5a**) additionally show an evolution of bands at 1354 cm⁻¹ and 1358 cm⁻¹ after infiltration, which are associated with the C-N vibrational A_{1g} mode. This indicates the formation of a bonding between Zn and N.^{30,31} Upon extension of the exposure time from 8 s to 120 s the C=N stretching mode of the quinoid units at 1492 cm⁻¹ vanishes and the C-C stretching band in the quinoid units at 1419 cm⁻¹ shifts. A blue shift of the 1168 cm⁻¹ band to 1183 cm⁻¹ after infiltration indicates a conversion of the already mentioned quinoid groups to benzenoid groups as the 1168 cm⁻¹ band is a signature of in plane C-H bending of quinoid units, while the 1183 cm⁻¹ band is attributed to the same mode in benzenoid units.³² A similar chemistry occurs upon doping the insulating EB to the conductive ES. The Raman spectra further shows the development of a small peak at 370 cm⁻¹, which becomes stronger pronounced with extended exposure times (red arrows in **Figure 5a**), and a shift of the ring deformation peak at 419 cm⁻¹ to 422 cm⁻¹, likely due to an embedded new contribution slightly above 419 cm⁻¹. Both newly occurring peaks fall into the spectral range where Zn-N bonds are expected to be seen and also indicate the formation of Zn-N bonds.³³ **Figure 5b** shows that with increasing Raman laser power the signature of ZnO at 568 cm⁻¹ (A₁ (LO) mode), 431 cm⁻¹ (E₂ mode) and 323 cm⁻¹ (2E₂(M)) can be detected.^{34,35} The Raman bands at 1360 cm⁻¹ and 1581 cm⁻¹ are assigned to D-(disordered) and G-(Graphitic) bands associated with the carbon-related defect complex,

respectively. These bands are characteristic for amorphous carbon materials,³⁶ indicating decomposition of PANI upon irradiation with high laser power.

Further information was gained from X-Ray diffractometry (XRD) and X-ray photoelectron spectroscopy (XPS). The XRD spectrum of the infiltrated polymer shows a peak at $2\theta=27.6^\circ$ (red arrow in **Figure 6a**), stemming from neither ZnO nor the EB. It can rather be assigned to the (111) reflection that is usually observed in acid doped PANI salts.³⁷ We chose a low number of cycles for identifying this peak, since a larger number of cycles results in more surface deposited ZnO and the resulting signal intensity increase, thus losing the sensitivity for this particular signal. As shown in **Figure 6b**, after 200 ZnO infiltration cycles, the characteristic peaks of PANI/ZnO appear at 31.76, 34.3, 36.21, 47.43, 56.5, 62.81 and 67.85 degrees, which can be indexed to the standard hexagonal wurtzite structure of ZnO.³⁸ No visible secondary phases or impurity peaks are observed.

The bonding states of nitrogen in PANI and ZnO-infiltrated PANI (120s, 5 cycles) were analyzed with XPS. PANI showed a nearly symmetric N 1s line centered around 399 eV (**Figure 7a**). This N 1s core spectrum consists of two peaks with equal intensity, centered at 398.44 eV and 399.71 eV. Those belong to the two chemically distinct nitrogen types in the imine (=N-) and amine (-NH-) fractions of the EB.³⁹ After infiltration (**Figure 7b**), the peak intensities of imine and amine type nitrogen significantly decrease, while at the same time a new component appears at 399.39 eV (moss green curve). This component can be assigned to Zn-bound nitrogen.

Doping of PANI is commonly done with Brønsted acids, which protonate the imine sites and create bipolarons that subsequently delocalize. Lewis acids can fulfill the same task by binding to the nitrogen. DEZ is a Lewis acid and our infiltration method implies a doping scheme similar to the common Lewis acid doping processes. However, upon single precursor infiltration of DEZ

or the even stronger Lewis acid trimethylaluminum (TMA), that is, without the use of the counter precursor H₂O, the conductivity of the infiltrated PANI did not rise. Thus, the water pulses play an important role. However, their application will result in a subsurface growth of ZnO. Composites with ZnO nanoparticles and acid doped PANI have been fabricated before, but their conductivities varied from 1.4×10^{-3} S/cm to 6.8×10^{-3} S/cm,¹⁷ significantly lower than those achieved with the infiltration strategy. It is intrinsic to the ALD process that the precursor binds covalently to the substrate, here the polymer backbone. The spectra show Zn being bound to the nitrogen in the polymer chain, while the application of water pulses will grow ZnO at the same time. In consequence, the formation of a ZnON-R type of hybrid phase is likely to occur. The resulting material can be seen from two perspectives, a Lewis acid doped PANI and a N-doped ZnO forming an interpenetrated hybrid network. The ZnO cross-linked polymer will provide additional conduction paths, but more importantly, the two components may mutually lower each other's band gap. This phenomenon is similar to the aluminum doped ZnO (AZO) and tin doped In₂O₃ (ITO), which usually show significant enhancement of conductivities of the base material after doping with Al or Sn.⁴⁰⁻⁴² In fact, doping with nitrogen is reported to reduce the band gap of ZnO from 3.4 eV to values between 1 and 2 eV in dependence of the doping level.⁴³ The dopant nitrogen in our system stems from the amine and imine groups of PANI, which upon binding to ZnO become oxidized and thus the doped units of the PANI backbone. This model is supported by the UV-Vis absorption spectra as shown in **Figure 8**. After infiltration, a new shoulder appears at 403 nm, which with 3.08 eV is much lower than the bandgap of ZnO. The band intensity at 453 nm, which corresponds to the π - π^* transitions in the benzenoid rings, increases, indicating a stronger presence of benzenoid units. The band at 625 nm that corresponds to the quinoid rings, decreases as a result of the conversion of quinoid rings to benzenoid rings (polaron

state). No obvious free-carrier tail was observed in the NIR region of the UV-Vis spectra.⁴⁴ This indicates that PANI cannot be considered as dominant charge promoter, but the hybrid system has to be considered as a whole. The N atoms donate electrons to the Zn atoms forming holes in the PANI main chain, which becomes a p-type semiconductor. ZnO is an n-type semiconductor, but the interfacial N-doped ZnO is known to be a p-type semiconductor, which results in a constellation similar to local *p-n* heterojunctions, which are dispersed over the whole system. Consequently, ZnO can drain the charge carriers from the PANI and no free-carrier tail is expected to occur. Therefore a resulting reaction scheme as depicted in **Figure 9** can be proposed.

CONCLUSION

Infiltration of polyaniline with ZnO from the vapor phase is an effective novel pathway for fabricating a conductive hybrid material. The conductivity of the material after infiltration is significantly beyond the additive contribution provided by the individual components. The reason for such improvement is most likely resulting from a synergistic effect induced by mutual doping of the inorganic and the polymeric constituents. The solvent-free processing enforces binding of Zn to the nitrogen present in the polymer backbone, which induces Lewis acid type of doping of PANI, while at the same time the ZnO becomes doped with nitrogen. The interpenetrated network further provides additional conduction pathways through crosslinking of the polymer chains with the inorganic material. With a large variety of semiconducting polymers being available, the process can easily be applied for the development of a plethora of further material combinations.

ASSOCIATED CONTENT

Supporting Information.

Supporting Information available: I-V plots of original PANI/ZnO (600 cycles) and PANI/ZnO (600 cycles) after storage in laboratory air for 6 months; TEM images with different magnification, SAED patterns and a HRTEM micrograph of a cross-sectioned ZnO-infiltrated PANI fiber (PANI/ZnO, 120 s, 155 °C, 200 cycles). All these supplemental materials can be available free of charge on the ACS Publications website at <http://pubs.acs.org>.

AUTHOR INFORMATION

Corresponding Author

*E-mail: qinyong@sxicc.ac.cn (Y. Qin)

*E-mail: m.knez@nanogune.eu (M. Knez)

Notes

The authors declare no competing financial interest.

ACKNOWLEDGMENT

W.W. and M.K. are grateful for funding from European Union FP7 Programme under grant agreement numbers 607232 (Marie Curie-ITN THINFACE) and 322158 (Marie Curie-CIG

ARTEN), and the Spanish Ministry of Economy and Competitiveness (MINECO) within grant agreement no. MAT2016-77393-R, including FEDER funds. Y.Q. appreciates the financial support from the Hundred Talent Program of the Chinese Academy of Sciences. C.C. thanks the Youth Innovation Promotion Association of the Chinese Academy of Sciences. The authors thank Dr. Jens Brede and Mikel Abadia for their support in XPS spectroscopy. The work was performed within the PCAM European doctorate. The authors acknowledge networking support within the COST action MP1402.

REFERENCES

1. Chiang, C. K.; Fincher, C.; Park, Y. W.; Heeger, A. J.; Shirakawa, H.; Louis, E. J.; Gau, S. C.; MacDiarmid, A. G. Electrical Conductivity in Doped Polyacetylene. *Phys. Rev. Lett.* **1977**, *39*, 1098-1101.
2. Yang, Y.; Westerweele, E.; Zhang, C.; Smith, P.; Heeger, A. J. Enhanced Performance of Polymer Light-Emitting Diodes using High-Surface Area Polyaniline Network Electrodes. *J. Appl. Phys.* **1995**, *77*, 694-698.
3. Kim, J. Y.; Lee, K.; Coates, N. E.; Moses, D.; Nguyen, T.; Dante, M.; Heeger, A. J. Efficient Tandem Polymer Solar Cells Fabricated by All-Solution Processing. *Science* **2007**, *317*, 222-225.
4. Klauk, H. Organic Thin-Film Transistors. *Chem. Soc. Rev.* **2010**, *39*, 2643-2666.
5. Li, D.; Huang, J. X.; Kaner, R. B. Polyaniline Nanofibers: A Unique Polymer Nanostructure for Versatile Applications. *Acc. Chem. Res.* **2009**, *42*, 135-145.
6. Pan, L. J.; Yu, G. H.; Zhai, D. Y.; Lee, H. R.; Zhao, W. T.; Liu, N.; Wang, H. L.; Tee, B. C. K.; Shi, Y.; Cui, Y.; Bao, Z. N. Hierarchical Nanostructured Conducting Polymer Hydrogel with High Electrochemical Activity. *Proc. Natl. Acad. Sci. USA* **2012**, *109*, 9287-9292.

7. Wang, W.; Chen, C.; Tollan, C.; Yang, F.; Qin, Y.; Knez, M. Efficient and Controllable Vapor to Solid Doping of the Polythiophene P3HT by Low Temperature Vapor Phase Infiltration. *J. Mater. Chem. C* **2017**, *5*, 2686-2694.
8. Huang, J.; Virji, S.; Weiller, B. H.; Kaner, R. B. Polyaniline Nanofibers: Facile Synthesis and Chemical Sensors. *J. Am. Chem. Soc.* **2003**, *125*, 314-315.
9. Wu, C. G.; Bein, T. Conducting Polyaniline Filaments in a Mesoporous Channel Host. *Science* **1994**, *264*, 1757-1759.
10. Huang, J. X.; Kaner, R. B. Nanofiber Formation in the Chemical Polymerization of Aniline: a Mechanistic Study. *Angew. Chem., Int. Ed.* **2004**, *43*, 5817-5821.
11. Lee, K.; Cho, S.; Park, S. H.; Heeger, A. J.; Lee, C. W.; Lee, S. H. Metallic Transport in Polyaniline. *Nature* **2006**, *441*, 65-68.
12. Chen, S. A.; Lin, L. C. Polyaniline Doped by the New Class of Dopant, Ionic Salt: Structure and Properties. *Macromolecules* **1995**, *28*, 1239-1245.
13. Chaudhuri, D.; Kumar, A.; Rudra, I.; Sarma, D. D. Synthesis and Spectroscopic Characterization of Highly Conducting BF₃-Doped Polyaniline. *Adv. Mater.* **2001**, *13*, 1548-1551.
14. Wang, W.; Yang, F.; Chen, C.; Zhang, L.; Qin, Y.; Knez, M. Tuning the Conductivity of Polyaniline through Doping by Means of Single Precursor Vapor Phase Infiltration. *Adv. Mater. Interfaces.* **2017**, *4*, 1600806.

15. Dimitriev, O. P. Doping of Polyaniline by Transition-Metal Salts. *Macromolecules* **2004**, *37*, 3388-3395.
16. Matnishyan, A. A. Synthesis and Study of Polyaniline Nanocomposites with Metal Oxides. *Phys. Solid State* **2011**, *53*, 1727-1731.
17. Mostafaei, A.; Zolriasatein, A. Synthesis and Characterization of Conducting Polyaniline Nanocomposites Containing ZnO Nanorods. *Prog. Nat. Sci.* **2012**, *22*, 273-280.
18. Manners, I. Putting Metals into Polymers. *Science* **2001**, *294*, 1664-1666.
19. Sanchez, C.; Julián, B.; Belleville, P.; Popall, M. Applications of Hybrid Organic–Inorganic Nanocomposites. *J. Mater. Chem.* **2005**, *5*, 3559-3592.
20. Houbertz, R.; Domann, G.; Schulz, J.; Olsowski, B.; Fröhlich, L.; Kim, W. S. Impact of Photoinitiators on the Photopolymerization and the Optical Properties of Inorganic–Organic Hybrid Polymers. *Appl. Phys. Lett.* **2004**, *84*, 1105-1107.
21. Gregorczyk, K.; Knez, M. Hybrid Nanomaterials through Molecular and Atomic Layer Deposition: Top down, Bottom up, and In-between Approaches to New Materials. *Prog. Mater. Sci.* **2016**, *75*, 1-37.
22. Lee, S. M.; Pippel, E.; Gösele, U.; Dresbach, C.; Qin, Y.; Chandran, C. V.; Bräuniger, T.; Hause, G.; Knez, M. Greatly Increased Toughness of Infiltrated Spider Silk. *Science* **2009**, *324*, 488-492.

23. Lee, S. M.; Pippel, E.; Moutanabbir, O.; Gunkel, I.; Thurn-Albrecht, T.; Knez, M. Improved Mechanical Stability of Dried Collagen Membrane after Metal Infiltration. *ACS Appl. Mater. Interfaces* **2010**, *2*, 2436-2441.
24. Gregorczyk, K. E.; Pickup, D. F.; Sanz, M. G.; Irakulis, I. A.; Rogero, C.; Knez, M. Tuning the Tensile Strength of Cellulose through Vapor-Phase Metalation. *Chem. Mater.* **2015**, *27*, 181-188.
25. Jur, J. S.; Parsons, G. N. Atomic Layer Deposition of Conductive Coatings on Cotton, Paper, and Synthetic Fibers: Conductivity Analysis and Functional Chemical Sensing Using “All-Fiber” Capacitors. *Adv. Funct. Mater.* **2011**, *21*, 1993-2002.
26. Sinha, S.; Sarkar, S. K. Atomic Layer Deposition of Textured Zinc Nitride Thin Films. *RSC Adv.*, **2014**, *4*, 47177-47183.
27. Michael, R. J. V.; Sambandam, B.; Muthukumar, T.; Umopathy, M. J.; Manoharan, P. T. Spectroscopic Dimensions of Silver Nanoparticles and Clusters in ZnO Matrix and Their Role in Bioinspired Antifouling and Photocatalysis. *Phys. Chem. Chem. Phys.*, **2014**, *16*, 8541-8555.
28. Shin, W. H.; Hwang, T. H.; Huh, Y. S.; Choi, J. W. Electrochemically Controlled Nanopore and Crystal Structure Evolution in Zinc Oxide Nanorods. *J. Electrochem. Soc.*, **2012**, *159*, A2143-A2147.
29. Alvi, F.; Ram, M. K.; Gomez, H.; Joshi, R. K.; Kumar, A. Evaluating the Chemio-Physio Properties of Novel Zinc Oxide–Polyaniline Nanocomposite Polymer Films. *Polym. J.* **2010**, *42*, 935-940.

30. Kim, S. J. A Surface Chemical Reaction in Organic–Inorganic Materials Using a New Chemical Evaporation System. *Chem. Mater.* **2015**, *27*, 4546-4551.
31. Reed, R. A. Resonance Raman Characterization of the Radical Anion and Triplet States of Zinc Tetraphenylporphine. *J. Phys. Chem.* **1991**, *95*, 9720-9727.
32. Louarn, G.; Lapskowski, M.; Quillard, S.; Pron, A.; Buisson, J. P.; Lefrant, S. Vibrational Properties of Polyanilines Isotope Effects. *J. Phys. Chem.* **1996**, *100*, 6998-7006.
33. Socrates, G. *Infrared and Raman Characteristic Group Frequencies: Tables and Charts*; West Sussex: John Wiley & Sons, 2007.
34. Hsu, C. H. Effect of the Cu Source on Optical Properties of CuZnO Films Deposited by Ultrasonic Spraying. *Materials* **2014**, *7*, 1261-1270.
35. Kaschner, A.; Haboeck, U.; Strassburg, M.; Strassburg, M.; Kaczmarczyk, G.; Hoffmann, A.; Thomsen, C. Nitrogen-Related Local Vibrational Modes in ZnO:N. *Appl. Phys. Lett.* **2002**, *80*, 1909-1911.
36. Artamonov, V. V.; Klyui, N. I.; Melnik, V. P.; Romanyuk, B. N.; Valakh, M. Ya.; Vasilik, O.; Semenovich, V. A.; Pérez-Rodríguez, A.; Morante, J. R. Micro-Raman and Microhardness Study of Nitrogen Implanted Diamond-Like Carbon Films. *Carbon* **1998**, *36*, 791-794.
37. Pouget, J. P. X-ray Structure of Polyaniline. *Macromolecules* **1991**, *24*, 779-789.
38. Verma, N. K. Effect of Zinc Oxide Nano Particle Concentration in the Polyaniline-Zinc Oxide Nanocomposite on the Dielectric Property. *Mater. Sci. Res. India* **2014**, *11*, 146-152.

39. Mahat, M. M. Elucidating the Deprotonation of Polyaniline Films by X-ray Photoelectron Spectroscopy. *J. Mater. Chem. C* **2015**, *3*, 7180-7186.
40. Hagendorfer, H.; Lienau, K.; Nishiwaki, S.; Fella, C. M.; Kranz, L.; Uhl, A. R.; Jaeger, D.; Luo, L.; Gretener, C.; Buecheler, S.; Romanyuk, Y. E.; Tiwari, A. N. Highly Transparent and Conductive ZnO: Al Thin Films from a Low Temperature Aqueous Solution Approach. *Adv. Mater.* **2014**, *26*, 632–636.
41. Lee, D. J.; Kim, H. M.; Kwon, J. Y.; Choi, H.; Kim, S. H.; Kim, K. B. Structural and Electrical Properties of Atomic Layer Deposited Al-Doped ZnO Films. *Adv. Funct. Mater.* **2011**, *21*, 448–455.
42. Cheun, H.; Fuentes-Hernandez, C.; Shim, J.; Fang, Y.; Cai, Y.; Li, H.; Sigdel, A. K.; Meyer, J.; Maibach, J.; Dindar, A.; Zhou, Y.; Berry, J. J.; Bredas, J. L.; Kahn, A.; Sandhage, K. H.; Kippelen, B. Oriented Growth of Al₂O₃:ZnO Nanolaminates for Use as Electron-Selective Electrodes in Inverted Polymer Solar Cells. *Adv. Funct. Mater.* **2012**, *22*, 1531–1538.
43. Lee, E.; Benayad, A. Nanocrystalline ZnON; High Mobility and Low Band Gap Semiconductor Material for High Performance Switch Transistor and Image Sensor Application. *Sci. Rep.* **2014**, *4*, No. 4948.
44. Xia, Y. N.; Wiesinger, J. M.; MacDiarmid, A. G. Camphorsulfonic Acid Fully Doped Polyaniline Emeraldine Salt: Conformations in Different Solvents Studied by an Ultraviolet/Visible/Near-Infrared Spectroscopic Method. *Chem. Mater.* **1995**, *7*, 443–445.

Figures and Figure Captions

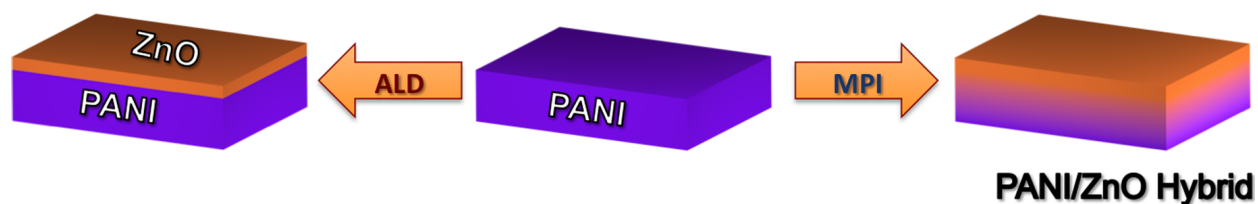


Figure 1. Schematic indicating the different resulting types of composites once a polymer is processed by atomic layer deposition (ALD) or multiple pulsed infiltration (MPI). With MPI the substrate is exposed to vapors of DEZ and H_2O in a sequential manner. Extended exposure times enable the precursors to diffuse into the polymer and react with the molecular backbone in the subsurface area forming a polymer-inorganic hybrid with a concentration gradient depending on the duration of exposure.

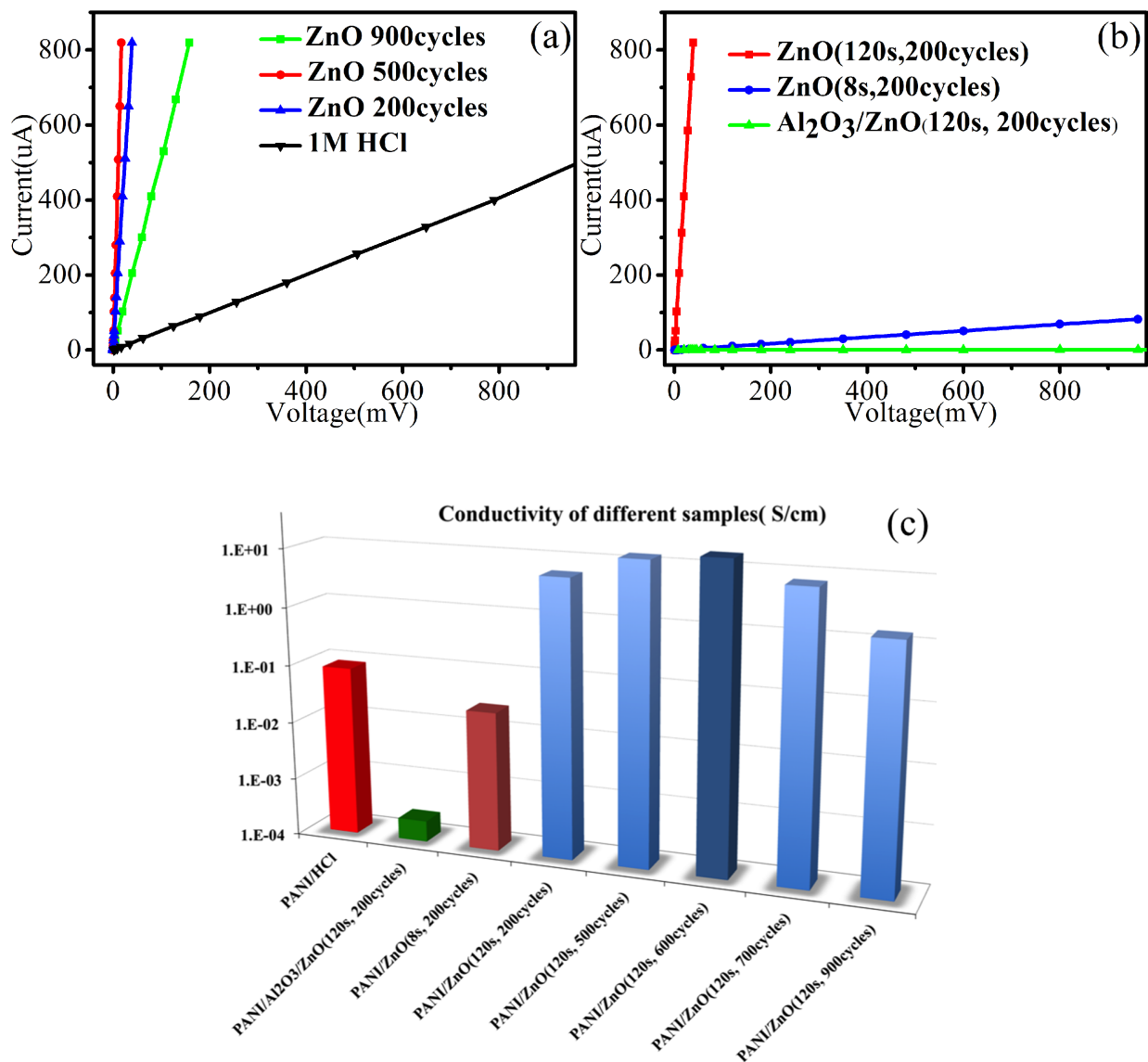


Figure 2. (a) *I-V* plots of PANI doped with 1M HCl (reference) and PANI doped with various numbers of infiltration cycles as indicated. The exposure time was 120 s per cycle in all cases. (b) *I-V* plots of PANI with a coating stack of Al₂O₃ (infiltration barrier)/ZnO, and PANI doped with ZnO applying short (8 s) and long (120 s) exposure times. The number of infiltration cycles

was fixed to 200 in all cases. (c) Comparison of conductivities of PANI after doping with HCl, coating with ZnO and infiltration with ZnO with varying exposure times and cycle numbers.

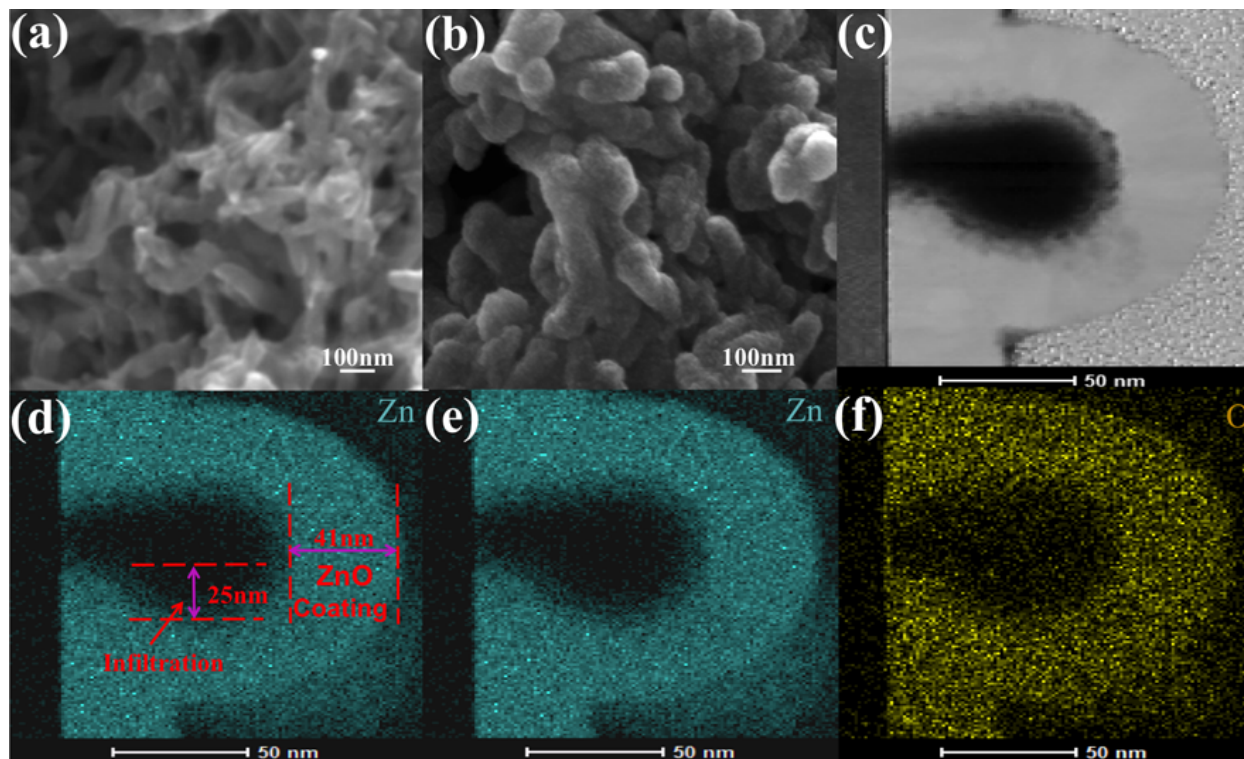


Figure 3. (a) and (b) SEM images of PANI and PANI/ZnO (120 s, 200 cycles). (c) TEM images of a cross-sectioned ZnO-infiltrated PANI fiber (PANI/ZnO, 120 s, 200 cycles), as prepared by the focused ion beam technique. (d) Zn elemental mapping of the cross-sectioned region with Zn infiltration and ZnO coating label. (e) Zn elemental mapping of the cross-sectioned region without label. (f) O elemental mapping of the cross-sectioned region.

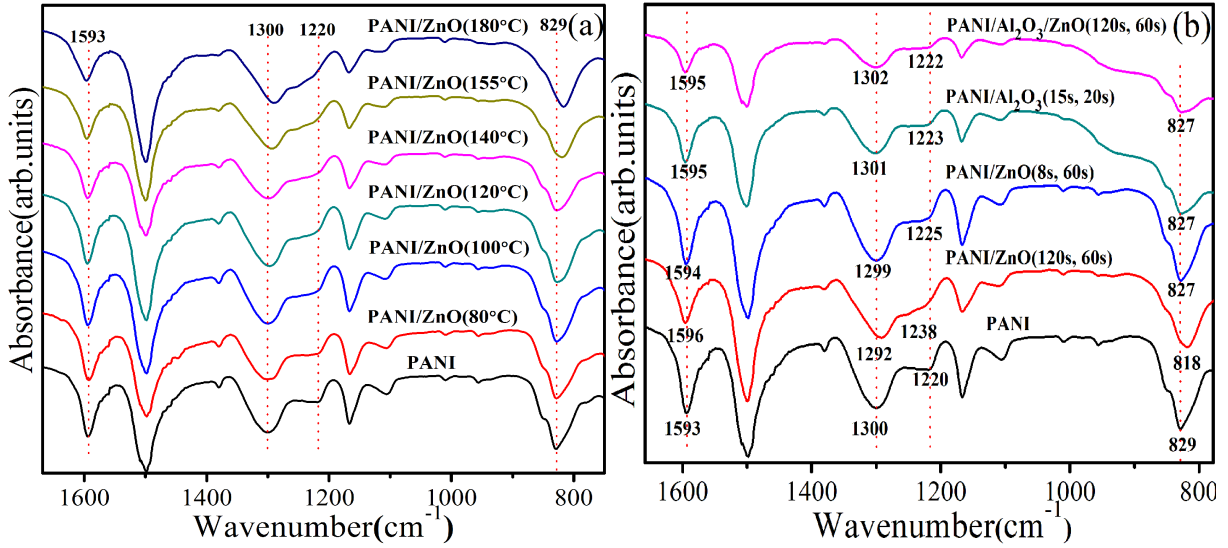


Figure 4. (a) FT-IR absorption spectra of PANI infiltrated with ZnO applying 120 s exposure time and 5 infiltration cycles. PANI emeraldine base was used as reference (black) and infiltration was performed at various temperatures from 80 °C to 180 °C. (b) FT-IR absorption spectra of PANI processed at 155 °C with various process settings: PANI control sample (black), ZnO-infiltrated with 120 s exposure time and 5 processing cycles (red), ZnO-infiltrated with 8s exposure time and 5 processing cycles (blue), PANI pre-coated with Al₂O₃ with exposure times of 15 s and 10 processing cycles (cyan) and Al₂O₃-coated PANI infiltrated with ZnO with 120 s exposure time and 5 processing cycles (magenta).

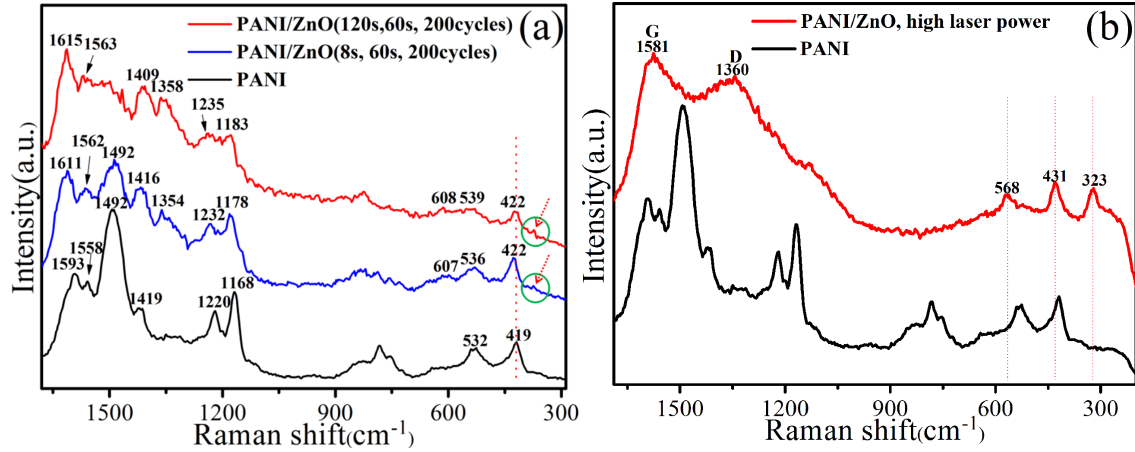


Figure 5. (a) Raman spectra of PANI (black), ZnO-infiltrated PANI with short exposure times (blue) and long exposure times (red) and process parameters as indicated in the figure. (b) Raman spectra of PANI (black) and PANI/ZnO (120 s, 60 s, 200 cycles, 155 °C) (red) under high Raman laser power.

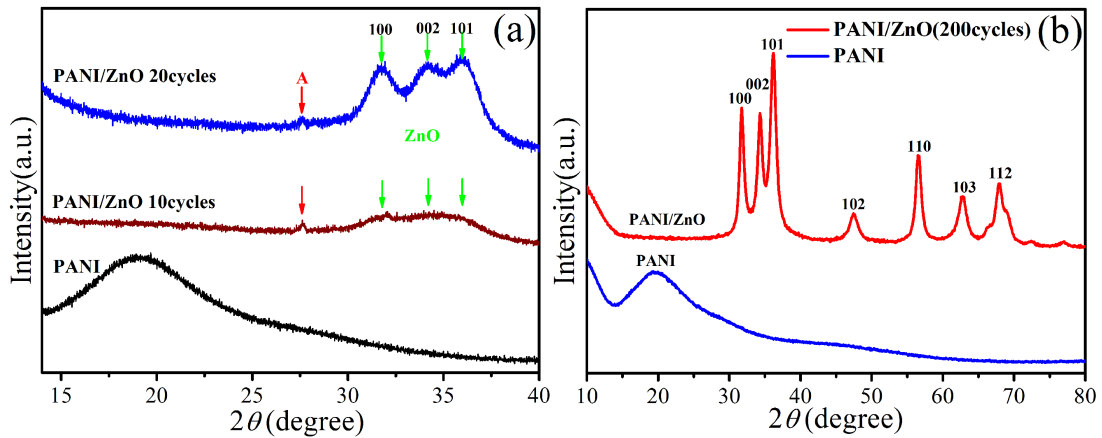


Figure 6. (a) XRD spectra of PANI before and after infiltration with 10 and 20 cycles ZnO applying 120 s exposure time. (b) XRD spectra of PANI control and PANI/ZnO (200 cycles).

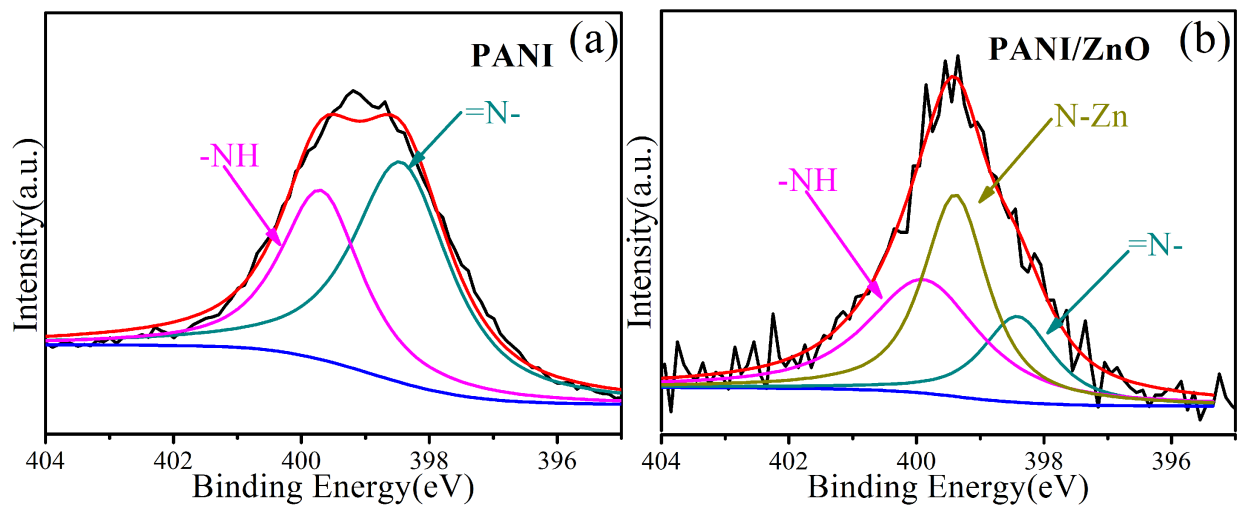


Figure 7. (a) N 1s XPS spectrum of PANI. (b) N 1s XPS spectrum of PANI infiltrated with ZnO applying 120 s exposure time and 5 processing cycles.

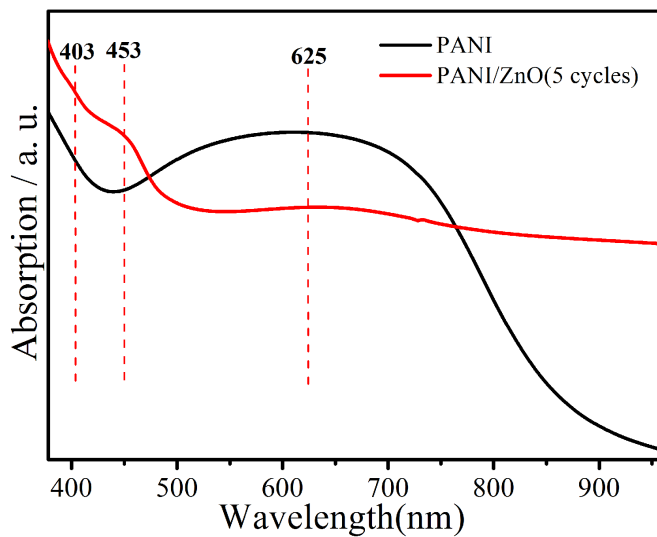


Figure 8. UV-Vis absorption spectra of PANI (black) and ZnO-infiltrated PANI applying 5 infiltration cycles and 120 s exposure time at 155 °C.

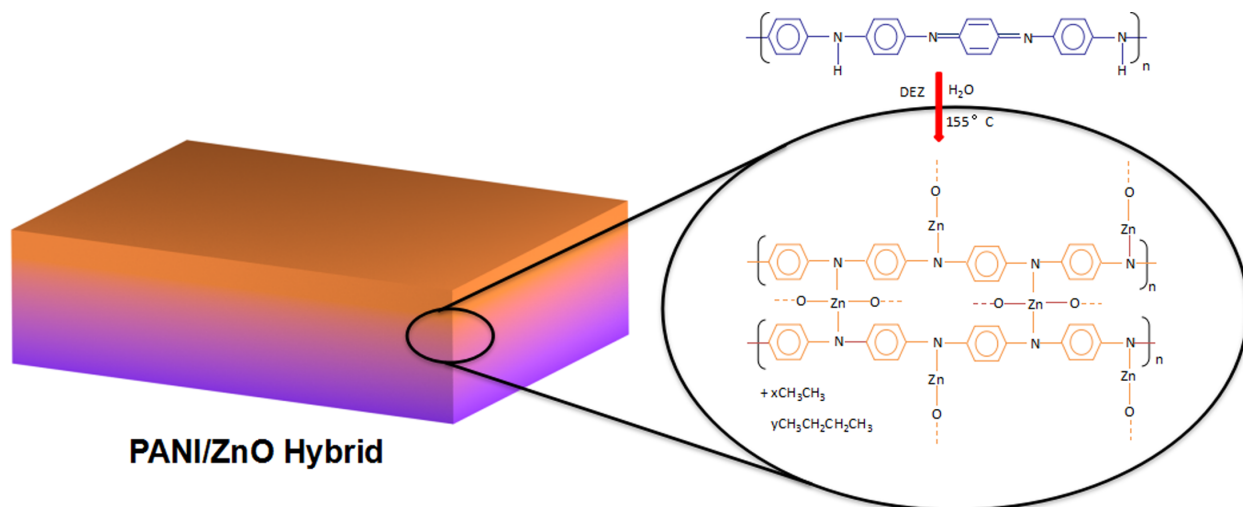


Figure 9. Macroscopic view on the hybrid material with covalently linked N-doped ZnO and Lewis acid doped PANI. Idealized schematic view of the chemical binding of Zn to the PANI backbone upon infiltration. The polymer chains become cross-linked with Zn-N bonds. While at the same time quinoid groups become benzenoid groups.

Table of Content Graphic

